Large Eddy Simulation-Probability Density Function modelling of nucleation and condensation of DBP droplets in a turbulent jet

N. Seubert, A. Kronenburg *, O. T. Stein

Institut für Technische Verbrennung, University of Stuttgart, Herdweg 51, 70174 Stuttgart, Germany

Y. Ge, M.J. Cleary **

The University of Queensland, School of Mechanical and Mining Engineering, QLD 4072, Australia

Abstract

Homogeneous nucleation and growth of dibutyl phthalate (DBP) droplets forming in a turbulent jet are modelled using LES combined with a probability density function/Monte Carlo method. LES resolves the largest turbulence structures but small scale processes like droplet nucleation and growth require closure. The Monte Carlo particles represent the gas temperature and species mass fractions, as well as the particle size distribution (PSD) of the DBP droplets. Thus all nucleation and growth terms are in closed form and the Interaction by Exchange with the Mean (IEM)-mixing model is used to account for the scalar mixing of the particles within each LES cell. The (physical) particle ensemble is represented by discrete size bins on each (stochastic) Monte Carlo particle. The LES-PDF method reproduces the experimental data well, and an analysis of the nucleation and growth terms demonstrates that the correlations of the large turbulent scales must not be ignored when modelling the averaged nucleation rate. In contrast, the large scale correlations do not significantly affect the particle growth, but the small scale, LES-subgrid term notably reduces particle growth for a wide particle size range.

Introduction

In industrial applications the knowledge and control of the particle size distribution (PSD) can be of primary concern for the improvement of the product quality or for pollutant minimization if particle formation needs to be avoided. The influence of natural particle sources such as volcano eruptions and large fires on the environment can also be better understood if the PSD is known. Most of the processes –let them be natural or industrial– are governed by turbulent fluid motion, and it is to be expected that the turbulence directly affects any small scale process such as particle nucleation and growth. Thus, the knowledge of turbulence-nucleation and turbulence-growth interactions is of major interest.

Experiments can provide valuable insights into the physics of particle dynamics [1, 2, 3] but they are limited by possible interferences with reactive environments and by the resolution of the employed measurement techniques, particularly at the nano-scale. Due to health constraints experiments on nanoparticle formation might require clean room environments which will then significantly increase the experimental cost. Therefore numerical simulations are a useful, cheap and risk-free means of extending the range of analysis beyond the experimental capabilites.

Polydispersed particulate flows can formally be described by the population balance equation (PBE) which requires closure, and a recent review on modelling techniques pertaining to the PBE can be found in [4]. The major approaches for the solution of the PBE are analytical and perturbation methods, moment and approximate moment-based methods, discretization and global approximation methods and the Monte-Carlo approach.

The literature on nanoparticle simulation research is vast, and we only briefly mention a selected number of references here, while a comprehensive review of the state-of-the-art can be found in [4]. Tsantilis et al. [16] used a moving sectional model to simulate flame synthesis of titania nanoparticles. Morgan et al. [17] simulated nanoparticle coagulation, sintering, particle inception and surface growth of a zero-dimensional system with a stochastic particle method. Mitchell & Frenklach [18] carried out detailed Monte Carlo simulations of particle aggregation and surface growth in the absence of fluid flow. Dang & Swihart [19] presented a two-dimensional model of silicon nanoparticle synthesis including the effects of fluid dynamics, laser heating, chemical reactions and all relevant processes of aerosol dynamics and compared the results from a moment method with those from a

*Corresponding author: kronenburg@itv.uni-stuttgart.de

**Current address: University of Sydney, NSW 2006, Australia

sectional model for a tubular reactor. Wang & Garrick [20] carried out 2D-DNS auf TiO_2 nanoparticle formation in a transient mixing layer based on a sectional approach.

Most relevant for the present work are studies by Garmory and Mastorakos [5] and Di Veroli and Rigopoulos [7]. Garmory and Mastorakos [5] used a Stochastic Fields transported Probability Density Function (PDF) method while Di Veroli and Rigopoulos [7] employed a Monte Carlo (MC) particle –PDF method [6]. The latter authors combined their MC/PDF method with a Reynolds Averaged Navier-Stokes (RANS)-based flow solver for the modelling of the evolution of the PBE in a turbulent flow. Lagrangian MC particles can provide information equivalent to the PDF transport equation, but at a cost which scales only linearly with the dimensionality of the joint-PDF. This linear scaling makes the calculation of the PDF of a high-dimensional system possible with current computer resources. Garmory & Mastorakos [5] and Di Veroli & Rigopoulos [7] applied their models to a turbulent round jet laden with dibutyl phthalate (DBP), that was examined experimentally by Lesniewski & Friedlander [1]. This setup facilitates model development and validation since the jet configuration yields a relatively simple flow field, DBP droplets are liquid and complex shapes of agglomerates do not need to be considered. In the current study the MC particle method is combined with large eddy simulations (LES) to model turbulent droplet nucleation and condensation, and it is then applied to the Lesniewski jet.

Experimental configuration

In the experiments conducted by Lesniewski and Friedlander [1] a hot nitrogen jet laden with DBP was used to study the nucleation and condensation processes. The nozzle was surrounded by an insulation layer and engulfed by a co-flow of air at ambient conditions. Turbulent mixing between the two streams of different temperature and composition evoked supersaturation and in turn homogeneous droplet nucleation and condensation. While the co-flow remained unaltered during the experimental campaign ($u_{co} = 0.18$ m/s, $T_{co} = 299$ K) various properties of the jet were studied. Inlet mole fractions of DBP in the range $1.1 \cdot 10^{-4} < x_{DBP,jet} < 5.2 \cdot 10^{-4}$, various bulk velocities and two nozzle diameters were used, while the jet was kept at a constant temperature T_{jet} = 413 K. The available datasets include measurements of the zeroth moment (total concentration of particles), the PSD, the mean particle diameter, the particle formation rate and the vapor concentration of DBP as functions of the Reynolds number and of the inlet DBP concentrations for various downstream locations along the jet centerline. In this paper we study the experimental conditions specified in [15] as *trial 824*. The conditions are u_{jet} = 51.55 m/s, T_{jet} = 413 K, $x_{DBP,jet} = 3.6 \cdot 10^{-4}$ with a nozzle diameter D_{noz} = 0.00235 m.

LES-MC modelling of turbulent particulate flows

Large eddy simulation is used to describe the time evolution of the largest turbulent structures. The Favre-filtered conservation equations of mass and momentum are solved, and the Smagorinsky model is used to close the subgrid stresses. The particle phase is governed by the Population Balance Equation [8]

$$\frac{\partial N(d_p,\vec{x},t)}{\partial t} + \nabla[\vec{u}\cdot N(d_p,\vec{x},t)] + \frac{\partial}{\partial d_p}[G(d_p,\vec{Y})\cdot N(d_p,\vec{x},t)] = D_p\nabla^2 N(d_p,\vec{x},t) + \dot{\omega}_N(\vec{Y},N) \tag{1}$$

where d_p, $\vec{x}$, t and $\vec{Y}$ denote the particle diameter, particle position, time and species mass fractions. N is the particle number density, $\vec{u}$ the velocity vector, G the particle growth rate, D_p the particle diffusivity and $\dot{\omega}_N$ denotes particle source terms to account for -in the general case- nucleation, aggregation and break-up. If the joint-PDF of species concentrations, temperature and the PSD is to be obtained, the dimensionality of the problem will prohibit an Eulerian solution of eq. (1) with the current computational resources. An equivalent solution of Fokker-Planck type equations like eq. (1) can be provided by solving a system of Langevin equations for the variables describing the properties of interest [9]. Therefore, we solve the Langevin equations for a representative number of stochastic Monte-Carlo particles

$$d\vec{x} = \vec{\tilde{u}}(\vec{x},t)\cdot dt + (2\cdot\Gamma(\vec{x},t))^{\frac{1}{2}}\cdot d\vec{\omega} \tag{2}$$

$$d\Phi_i = [M(\vec{x},\Phi_i) + W_i(\Phi)]dt \tag{3}$$

where eq. (2) describes the particle motion in turbulent flow, Γ is the effective diffusivity and $d\vec{\omega}$ denotes the increment of a Wiener process with zero mean and variance $\sqrt{\Delta t}$. Equations (3) describe the time evolution of $i = 1...n$ transported scalars Φ_i, M is the mixing operator and W_i are the scalar source/sink terms. To model DBP nucleation and condensation the Φ_i include temperature, the species mass fractions of DBP, O_2 and N_2 and 30 size bins to represent the discrete PSD. The turbulent mixing described by M requires modelling and we use the

simple IEM mixing model [10] in this paper. In contrast to Eulerian solution approaches for the PBE, where the subgrid contribution is unknown, the information carried by the stochastic particles is locally exact and therefore the source/sink terms W_i appear in closed form (cf. our discussion in Section *Results and Discussion*). The reader should note that temperature and all gas phase species mass fractions are *also* computed on the LES grid by the Favre filtered equations. These are redundant information and only used for comparison with the corresponding particle solutions and for the computation of B_2 and B_3 in Section *Results and Discussion*. The temperature source term accounts for the latent heat of phase change, which is assumed to be small and neglected here. This avoids a two-way coupling between gas-phase and particles, but may be responsible for the over-prediction of the nucleation rates, as reflected in the droplet number concentration m_0 for $z/D > 20$ shown later. The correct treatment of the latent heat, mass loss of the gas phase due to condensation and a full two-way coupling will be considered in the future work. The source/sink terms for the discrete particle size bins describe droplet nucleation and growth. Homogeneous nucleation occurs at the critical diameter

$$d_{p,cr} = \frac{4\sigma v_m}{kTln(S)} \tag{4}$$

where σ, v_m, k, T, and S are the surface tension, molecular volume, Boltzmann constant, temperature and the saturation ratio, respectively. The functional dependence of the surface tension on temperature is represented by the expression in [7]. The saturation ratio is calculated as $S = P_{DBP}/P_{sat}$, with the DBP partial pressure P_{DBP} and the saturation pressure P_{sat}, which is modelled according to [5]. The nucleation rate B can be written as [11]:

$$B(S,\sigma,T) = \frac{N_v^2 v_m}{S}\left(\frac{2\sigma}{\pi m}\right)^{\frac{1}{2}} exp\left(-\frac{16\pi\sigma^3 m^2}{3(kT)^3\rho_l^2(ln(S))^2}\right) exp\left(\frac{s_{mon}\sigma}{kT}\right) \tag{5}$$

with the vapor concentration N_v [molecules/m^3], the mass of a monomer/molecule m, the liquid density ρ_l and the surface area of a monomer s_{mon}.

Droplet growth is considered as follows: According to [7] the experimental Knudsen number $\text{Kn} = 2l_p/d_p$, where l_p denotes the mean free path of the gas molecules, ranges from very large numbers for nucleating particles to $\text{Kn} \approx 1$ for the largest droplets and hence, droplet growth both in the free molecular and continuum regimes should be considered. Following [7] we use the approximate formula of Fuchs & Sutugin [14] for the entire Knudsen number range, which modifies the growth rate expression for the continuum regime by a corrective coefficient $\alpha(\text{Kn}) = (1+\text{Kn})/(1+1.71\text{Kn}+1.333\text{Kn}^2)$ to yield

$$G_{d_p} = \alpha(\text{Kn}) \cdot \frac{4Dv_m P_{sat}}{kTd_p}(S-1) \tag{6}$$

with the molecular diffusivity D. According to [7] the characteristic particle collision time scale for the highest inlet mole fraction of DBP ($x_{DBP,jet} = 5.2 \cdot 10^{-4}$) used in the experiments is $\tau_{coll} = 100$s. This is by far larger than the time of any process considered here, thus particle collision/aggregation is neglected in [7] and the present simulations.

Computational Parameters

The simulations are carried out with the OpenFOAM toolbox, v2.1.x, which was extended for the present PBE-LES of DBP condensation. The simulation domain is a cylinder with a length of 53 nozzle diameters and a radial extent of 23 diameters. The nozzle is resolved with 17 cells resulting in a minimum mesh width of 138 μm. The bluff body resulting from the nozzle insulation layer is discretised with 21 cells, which yields a cell size of 580 μm across the bluff body. Considerable stretching in axial direction is used to cluster cells in the upstream region where an adequate resolution is crucial for the initiation of nucleaction and to reduce the number of downstream cells. The boundary conditions for velocity and pressure are fixed value and zero gradient at the inlet and vice versa at the outlet. Zero gradient boundary conditions are used for all quantities at the lateral domain boundary. LES requires transient inlet conditions, and a mean velocity profile corresponding to the experimental bulk velocity is superimposed with inflow turbulence generated using the method by Kempf et al. [13]. A population control algorithm is implemented to keep the number of particles per LES cell at ≈ 5, which is a relatively low number for MC/PDF computations. This can be justified however, since averages are taken over several flow through times and all local, time averaged results presented here stem from sampling several thousands of particles.

Results and Discussion

Figure 1 gives an impression of the instantaneous flow and mixing fields, as well as the axial velocity statistics along the jet centerline. In Fig. 1(a) streamlines and a selected number of MC particles couloured by their temperature are jointly plotted in a 2D planar cut through the domain that includes the jet centerline.

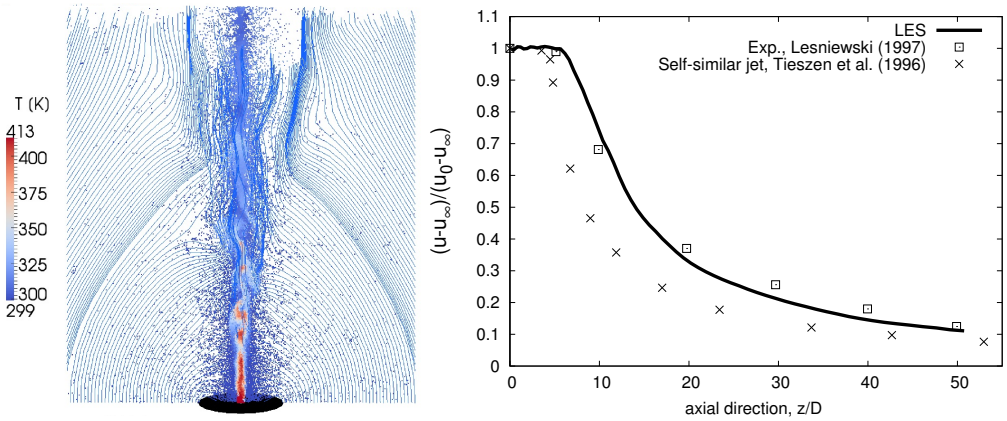

(a) streamlines and MC particle temperature (b) mean axial velocity along centerline

Figure 1. (a) Instantaneous 2D snaphot of the streamlines overlaid by a selected number of Monte-Carlo particles coloured by their temperature. A plane sheet of thickness 2 mm through the jet centerline was used to extract the MC particles for visualisation. (b) Comparison of the mean axial velocity along the centerline from LES, experiments by Lewsniewski [15] and the self-similar jet profile of Tieszen et al. [21]. The velocity u is normalised with the free-stream (co-flow) velocity u_∞ and the inlet centerline velocity u_0.

The insulation layer around the jet is shown in black. The insulation layer acts as a bluff-body in the co-flowing stream, which leads to recirculation of co-flow fluid towards the jet and upstream mixing of the two streams. Further downstream, mixing is due to turbulent jet break-up and entrainment of air from the lateral domain boundary. Mixing leads to cooling of the hot jet, which triggers supersaturation and homogeneous nucleation of DBP droplets. Figure 1(b) compares profiles of the mean axial velocity from LES with equivalent data from [15, 21] along the jet centerline. In LES, jet break-up is a strong function of the transient inflow conditions, and the break-up point can be controlled by adjusting the parameters of the inflow generator according to (measured) turbulence information. In the absence of such data the inflow was set to yield the approximate break-up behaviour and to represent best the mean velocity from the reference experiment [15] in the upstream region (z/D < 20), where most droplet statistics are available. In fig. 2 the time-averaged zeroth moment of the particle size distribution of DBP droplets along the jet centerline is shown.

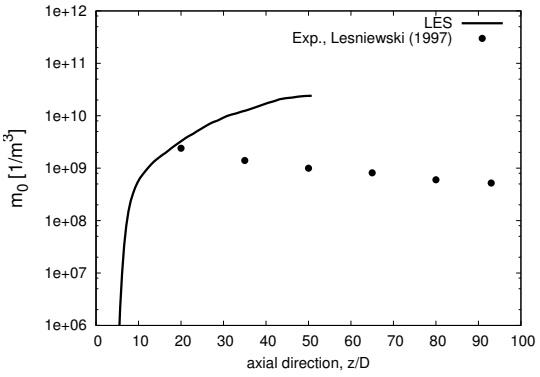

Figure 2. Comparison of the time-averaged zeroth moment m_0 of the PSD (number concentration of droplets per unit volume) along the jet centerline.

The mixing due to the turbulent jet break up at z/D = 6 leads to homogeneous nucleation and to a steep increase of particle number density. At z/D = 20 the zeroth moment obtained from the MC particles is similar to the experimental value given by [15]. However, the trend of a decreasing number particle density for z/D > 20 could not be reproduced in the current simulation, but is likely to occur beyond z/D = 50. The reader should note that the close match of experiments and LES at z/D = 20 may be somewhat fortuitous, and that a different choice of the models for surface tension and saturation pressure will lead to notable differences. Garmory and Mastorakos [5] demonstrated that a modification of the temperature dependence of the surface tension can affect the spatial evolution of the nucleation rate, but tuning has not been attempted here. The focus of the current paper is the qualitative assessment of the influence of turbulence on nucleation and growth. We analysed the results from computations using different models for saturation pressure, surface tension and nucleation: while the absolute values for nucleation and growth may differ significantly, the relative influence of turbulence on nucleation and growth does not vary much and trends reported here are quite insensitive to the exact closures used.

The effect of particle growth can be best assessed by comparison of the size distribution function. In Fig. 3 the logarithmic density distribution dN/dlog(d_p) obtained from the LES-PDF method is compared with the experimental values from [15] at z/D = 20. The figure shows the temporal averages from all MC particles at z/D = 20 with a position of r < 0.0025 m. This is to account for the size of the suction probe. Since no experimental PSD data for the inlet mole fraction $x_{DBP,jet}$ = $3.6 \cdot 10^{-4}$ is available, the computations are compared with data from experiments with $x_{DBP,jet}$ = $3.7 \cdot 10^{-4}$. The agreement of the simulations with the reference experiment is not fully satisfactory, with the simulation showing a monotonous increase of the population up to $d_p \approx 0.1\mu m$, followed by a steep negative slope (i.e. negligible numbers of large droplets), whereas the experiment shows overall less populated small size bins and considerably more large droplets. Similar difficulties occurred in the simulations by [7] and there a plug flow reactor model was used to post-process the data from the RANS-PBE simulation. This was done to mimick the additional droplet growth potentially happening inside the sampling apparatus, but no attempt has been made here to include such effects here.

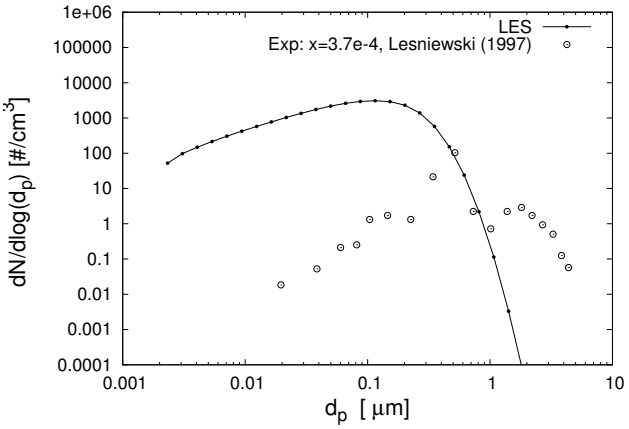

Figure 3. Comparison of the logarithmic density distribution dN/dlogd_p extracted at z/D=20.

We will now focus on the interactions between turbulence and particle nucleation and growth. They can be best assessed by evaluating the time averaged nucleation (B_i) and condensation (G_i) rates (eqs (5) and (6)) using different methods. Three methods are used here:

1. $B_1 \equiv \overline{B(S, \sigma(T), T, N_v)} \hat{=}$ time averaged nucleation rate computed from MC particle values
2. $B_2 \equiv \overline{B(\widetilde{S}, \sigma(\widetilde{T}), \widetilde{T}, \widetilde{N_v})} \hat{=}$ time averaged nucleation rate computed from LES-filtered values, and
3. $B_3 \equiv B(\overline{\widetilde{S}}, \sigma(\overline{\widetilde{T}}), \overline{\widetilde{T}}, \overline{\widetilde{N_v}}) \hat{=}$ time averaged nucleation rate computed from time averaged LES-filtered values.

The tilde denotes LES-filtered values, the overbar denotes time averaging. The Monte Carlo particles represent instantaneous solutions of the composition and the PBE, the effects of turbulence appear in closed form, and the time averages obtained from the MC particles (B_1) therefore converge towards the (correct) statistical mean. The time average B_2 is obtained from the LES-filtered values. The difference between B_1 and B_2 is therefore a measure

for the importance of the LES subgrid correlations that are neglected when computing B_2. Finally, B_3 is computed from the time-averaged LES-filtered values and corresponds to a solution that would be obtained from a RANS based approach without turbulence model for the solution of the PBE. Similarly, the supersaturations S_1, S_2 and S_3 and the growth terms G_1, G_2 and G_3 denote the particle solution, the solution without LES-subgrid correlations and the solution without turbulence effects in the RANS context, respectively.

Figure 4 shows contour plots of the time averaged homogeneous nucleation rates B_1, B_2 and B_3 in a 2D plane including the jet centerline, note the different scales. Clear qualitative differences can be observed. In particular a RANS based approach where turbulence interactions with the nucleation rate are neglected, would lead to large nucleation rates in the shear layer quite upstream while the particle method demonstrates a relatively low nucleation rate in the shear layer close to the nozzle and a predominant nucleation further downstream and closer to the centerline.

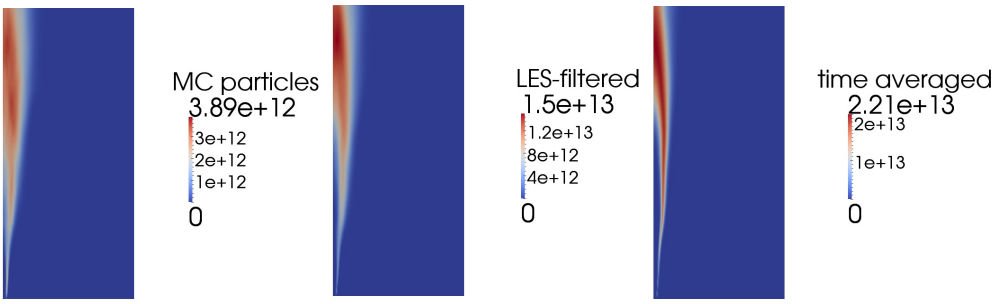

(a) (b) (c)

Figure 4. Comparison of the time-averaged nucleation rates: (a) B_1, (b) B_2 and (c) B_3.

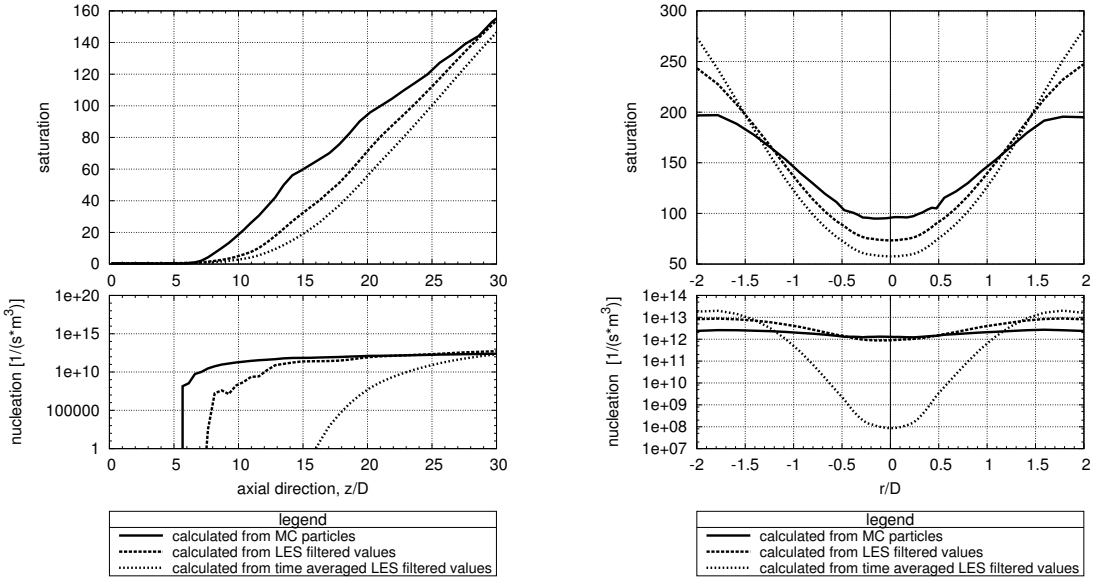

(a) (b)

Figure 5. Comparison of the time-averaged saturation ratios, $\overline{S}$, and nucleation rates $\overline{B}$, evaluated from the instantaneous, local particle information, the instantaneous, Favre-filtered LES data and the temporal LES-filtered averages values along (a) the jet centerline and (b) radius at z/D = 20.

Figure 5 allows for a better quantitative comparison. The top figures present the time-averaged saturation ratio S and the bottom figures show the time averaged nucleation rates B along (a) the jet centerline and (b) as a function

of the radial position at z/D = 20. While S_1 reaches significant values at the end of the potential core of the jet (z/D = 6), S_2 increases slightly further downstream and RANS-based data reveal an even greater delay. While the radial distribution of the saturation shows higher values in the shear layer for S_2 and S_3, the saturation calculated from the MC particles indicates an overall more uniform distribution. These observations are in agreement with [7]. The effects are similar but much stronger for the nucleation rates. Due to the non-linear dependence of B on supersaturation and mixing (temperature, vapour mole fraction and surface tension), differences can amount to five orders of magnitude! This indicates the significance of turbulence on particle production. The effects of small scale turbulence that are neglected in B_2 can be of the order of $O(10)$, the effects of large scale turbulence that are neglected in B_3 can amount to 5 orders of magnitude, $O(10^5)$. As indicated above, these findings are relatively insensitive towards the exact models used for saturation pressure, surface tension and nucleation rate.

Figure 6 shows the time-averaged condensation rates G_1, G_2 and G_3 along the jet centerline (a) and in cross-stream direction at different axial positions (b)-(d) for size bin 10. Here, size bin 10 represents particles with a diameter $d_p = 3.78 \times 10^{-8} m$, but the following observations are valid throughout all size bins.

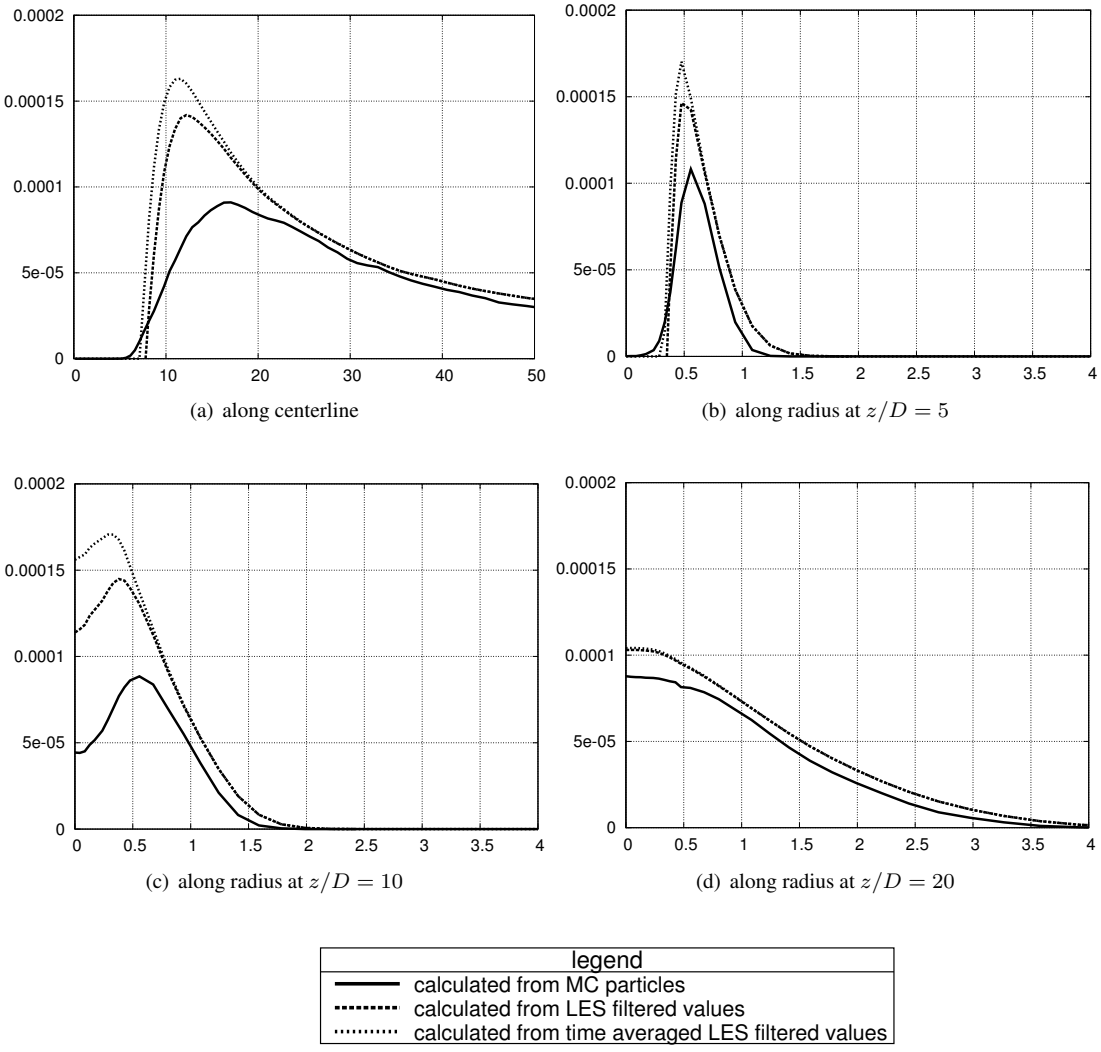

(a) along centerline

(b) along radius at $z/D = 5$

(c) along radius at $z/D = 10$

(d) along radius at $z/D = 20$

Figure 6. Condensation rate [m/sec] for size bin 10: Along the centerline (a), and the along radius at $z/D = 5$ (b), $z/D = 10$ (c) and $z/D = 20$ (d).

The comparison demonstrates the significance of the small scale turbulence on the particle growth process. Along the centreline, Fig. 6 (a), the highest condensation rate is obtained by calculations using the condensation rate based on RANS type values, G_3, followed by the rate based on the LES filtered values G_2 and the particle values G_1. This indicates that large scale mixing does not affect the growth mechanism too much, however, the small scale processes are extremely important and must not be neglected. However, the discrepancies between the

different approaches become increasingly less downstream. Along the radius, the same trends can be observed and the profiles show a peak of the condensation rate in the shear layer away from the axis for z/D $\leq$ 10, whereas at z/D = 20 maximum condensation occurs at the centerline.

Summary and Conclusions

Homogeneous nucleation and condensation of DBP droplets in a hot, turbulent nitrogen jet were simulated using a novel LES-MC/PDF approach. The predicted droplet number density was in good agreement with the experimental data, while simulation results for the particle size distribution showed some discrepancies. The emphasis has been placed on the correct modelling of the turbulence-nucelation and turbulence-growth interactions. These interactions appear in closed form when the MC/PDF method is used and do not require modelling. We have shown that the large turbulence scales have a significant effect on particle nucleation. Neglecting the large scale effects, nucleation rates can be underpredicted locally by up to 5 orders of magnitude while omission of the small scales tends to give an overprediction by one order of magnitude only. The growth terms are strongly affected by small scale turbulence instead, and the omission of the LES-subgrid correlations can lead to errors of one order of magnitude.

References

[1] T. K. Lesniewski and S. K. Friedlander, *Proc. Roy. Soc. Lond. A*, 454:2477-2504, 1998.
[2] A. Gupta, P. Ifeacho, C. Schulz and H. Wiggers, *Proc. Combust. Inst.*, 33:1883-1890, 2011.
[3] S.E Pratsinis, O. Arabi-Katbi, C.M. Megaridis, P.W. Morrison Jr., S. Tsantilis and H.K. Kammler *Mat. Sci. Forum*, 343-346:511-518, 2000.
[4] S. Rigopoulos, *Progr. Energy Combust. Sci.*, 36:412-443, 2010.
[5] A. Garmory and E. Mastorakos, *Chem. Eng. Sci.*, 63:4078-4089, 2008.
[6] S. B. Pope, *Combust. Sci. Technol.*, 25(5-6):74-159, 1981.
[7] G. Y. Di Veroli and S. Rigopoulos, *Phys. Fluids*, 23(4):043305, 2011.
[8] G. Y. Di Veroli and S. Rigopoulos, *AIChE Journal*, 56(4):878-892, 2010.
[9] C. W. Gardiner, *Handbook of Stochastic Methods*, Springer Verlag.
[10] J. Villermaux and J. C. Devillon, *2nd Int. Symp. Chem Reac. Eng.*, 1-13, 1972.
[11] S. L. Girshick and C. Chiu, *J. Chem. Phys.*, 93:1273, 1990
[12] S. K. Friedlander, *Smoke, Dust, and Haze*, Oxford University Press.
[13] A. Kempf, M. Klein, J. Janicka, *Flow Turbul. Combust.*, 74:67-84, 2005.
[14] N. A. Fuchs, A. G. Sutugin, *Topics in Current Aerosol Research* 2:1-60, 1971.
[15] T. K. Lesniewski, "Particle Nucleation and Growth in Turbulent Jets", *PhD thesis*, UCLA, USA, 1997.
[16] S. Tsantilis, H.K. Kammler, S.E. Pratsinis, *Chem. Eng. Sci.*, 57:2139-2156, 2002.
[17] N. Morgan, C. Wells, M. Kraft, W. Wagner, *Combust. Theo. Mod.*, 9(3):449-461, 2005.
[18] P. Mitchell, M. Frenklach, *Phys. Rev. E*, 67:061407, 2003.
[19] H. Dang, M.T. Swihart, *Aeros. Sci. Technol.*, 43(3):250-263, 2009.
[20] G. Wang, S.C. Garrick, *J. Aeros. Sci.*, 37, 431-451, 2006.
[21] S. R. Tieszen, D. W. Stamps and T. J. O'Hern, *Combust. Flame* 106:442-462, 1996.